110th Anniversary: Cellulose Nanocrystals as Organic Nanofillers for Cellulose Triacetate Membranes Used for Desalination by Pervaporation

by Indah Prihatiningtyas

Submission date: 17-Mar-2022 10:28AM (UTC+0700)
Submission ID: 1786083744
File name: cnc_di_IE_R_journal.pdf (7.33M)
Word count: 6474
Character count: 34283

I&EC research
Industrial & Engineering Chemistry Research

Article

Cite This: Ind. Eng. Chem. Res. 2019, 58, 14340−14349

pubs.acs.org/IECR

110th Anniversary: Cellulose Nanocrystals as Organic Nanofillers for Cellulose Triacetate Membranes Used for Desalination by Pervaporation

Indah Prihatiningtyas,[†,‡] Alexander Volodin,[§] and Bart Van der Bruggen*[,†,∥]

[†]Department of Chemical Engineering, KU Leuven, Celestijnenlaan 200F, B-3001 Leuven, Belgium

[‡]Department of Chemical Engineering, Mulawarman University, Jalan Sambaliung No. 9, Sempaja Selatan, Samarinda, Kalimantan Timur 75119, Indonesia

[§]Laboratory of Solid-State Physics and Magnetism, Department of Physics and Astronomy, K.U. Leuven, Celestijnenlaan 200D, B-3001 Leuven, Belgium

[∥]Faculty of Engineering and the Built Environment, Tshwane University of Technology, Private Bag X680, Pretoria 0001, South Africa

Supporting Information

ABSTRACT: Membranes with a high water flux and excellence in separating NaCl are required in pervaporation (PV) for water desalination. Cellulose nanocrystals (CNCs) are low cost and hydrophilic with good mechanical properties. Therefore, they could potentially enhance the water flux of PV membranes. Cellulose triacetate/cellulose nanocrystals (CTA/CNCs) nanocomposite PV membranes were successfully fabricated via solution casting, aiming to improve the water desalination performance. The effects of CNCs on the membrane morphology, hydrophilicity, mechanical properties, water flux, and rejection were investigated. Incorporating CNCs changed the membrane structure from spongelike to self-assembled structure. PV experiments showed incorporating 3% CNCs into a CTA membrane effectively enhanced the water flux by a factor of 3, from 2.16 kg m^{-2} h^{-1} to 5.76 kg m^{-2} h^{-1}. This was further optimized by reducing the casting blade height from 200 to 100 μm, thus obtaining a flux of 11.68 kg m^{-2} h^{-1}, while the NaCl rejection remained 99.9%. The CNCs 3%-CTA PV membrane with a casting blade height of 100 μm also showed a good performance for 12 h of separation. This newly developed PV membrane allows for an excellent separation of water from NaCl. Moreover, it has a substantially increased water flux compared to a pristine membrane and is thus potentially applicable for desalination.

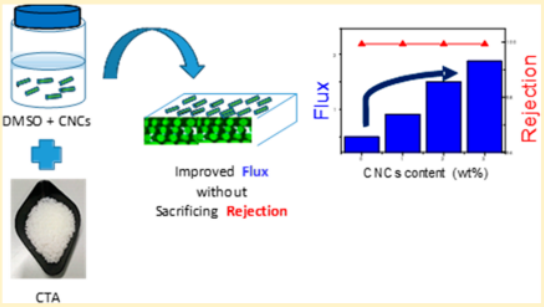

1. INTRODUCTION

Water scarcity has become one of the crucial issues in many parts of the world due to rapid population growth, industrialization, agriculture, water pollution, and climate change.[1,2] One of the strategies to elevate this issue is to use desalination technology. There are two major types of desalination processes: thermal desalination and membrane process separation. Thermal desalination includes multistage flash distillation (MSF), multiple effect distillation (MED), vapor compression (VC), freezing, humidification-dehumidification (HDH), and solar desalination whereas membrane processes include pressure-driven processes, electro-driven separation, and thermally driven membrane technology.[3−5]

Pervaporation (PV) is one of the thermal-driven membrane process which currently receives growing attention. PV uses dense hydrophilic membranes where difference partial vapor pressure across the membrane acts as separation driving force. The permeate side is usually kept lower than the partial pressure on the feed. Permeating vapor is removed by reducing the pressure and then collected after condensation.[6,7] PV is an activity-driven membrane process, which can be applied for seawater desalination due to the following advantages: (1) the salt selectivity for different membranes in PV is generally above 99%, (2) the hydrophilic properties of PV yields a superior antifouling property,[4] (3) it is an environmentally friendly process, and (4) PV is able to handle highly concentrated water without the need to adjust the vapor pressure difference across the membrane as the driving force, for example, for high salinity (400 g/L) in produced water in the oil and gas industry.[8−11]

Received: April 23, 2019
Revised: June 26, 2019
Accepted: July 4, 2019
Published: July 4, 2019

DOI: 10.1021/acs.iecr.9b02106
Ind. Eng. Chem. Res. 2019, 58, 14340−14349

As a thermal-driven process, PV requires relatively low electrical energy and thus can utilize a low-grade heat resource such as waste heat or heat recovered from industrial plants.[4,8] Furthermore, there is a possibility to employ renewable energy sources (geothermal energy or solar energy) when it can be effectively used to heat the feed to a certain temperature.[12,13] Nowadays, extensive efforts are made to obtain the optimal PV desalination membrane, which has the most efficient separation. PV membranes have been developed for desalination using various polymers, inorganic and polymer−inorganic hybrid materials. However, most PV membranes have a relatively low water flux when applied to desalination. Strategies to increase water flux of membranes, including enhancing membrane surface hydrophilicity in order to have a strong affinity for water molecules, promoting water transport through the membrane with lower mass transfer resistance by introducing nanomaterials, and decreasing the membrane thickness.[4]

Polymers are the most widely used materials for desalination. Polyethylene (PE) and cellulose are the two organic polymers that are widely used in the fabrication of PV membranes.[4] Cellulose is the most abundantly available material on the earth and renewable natural polymer. Cellulose triacetate (CTA) is a cellulose acetate-based material, which is considered an attractive polymer for membrane fabrication. Since the 1960s, CTA based membranes have been widely used in various applications due to the good mechanical properties of CTA, its competitive cost, relative hydrophilicity, and low fouling tendency. Moreover, CTA based membranes have a good performance in desalination; hence, cellulose triacetate (CTA) hollow fiber membranes have dominated the seawater desalination market in the Middle East compared to mainstream polyamide TFC RO membranes. CTA based membranes also have a better oxidation resistance, and can be fabricated into dense films.[14−21] Huth et al.[11] used a commercial CTA membrane (Hydration Technology Innovations, Scottsdale, AZ) for desalinating high-salinity brine (100 g/L) by pervaporation with a sweeping gas and obtained a water flux of 2.3 kg m^{-2} h^{-1} at 50 °C and a salt rejection >99%.[8]

A high water permeation and a high salt rejection are required for PV membranes, but most polymers have a limited permeability. This requires a large surface area, which increases the process cost. The salt rejection in PV is typically very high because of the nonvolatile character of salts. The advancement of material science led to the development of cost-effective PV desalination membranes with excellent separation properties. The incorporation of nanoparticles into the polymer matrix can lead to a significant improvement to overcome the drawbacks of the existing polymeric membranes, by increasing the water permeability, through an increased surface hydrophilicity, surface charge density, and by enhancing antifouling properties, the antibacterial effect, and chlorine resistance.[22−24] Commonly tested nanomaterials used as fillers for desalination membranes includes silica, zeolite, alumina, clay, TiO_2, GO, CNT, and MWNT.[25] Nevertheless, the major challenge of incorporating nanoparticles besides dispersing into polymer is leaching out into the permeate or retentate stream.[24] In addition, some commonly used nanoparticles are particularly costly and difficult to produce.[26−29] In this paper, the incorporation of cellulose nanocrystals (CNCs) in CTA PV membranes was investigated to enhance the water flux. CNCs are a white odorless crystalline dry powder; they are a renewable material with low cost and abundant as raw material.[30,31] CNCs are explored as an alternative to improve mechanical properties, with low weight and a large specific surface area. In a broader context, CNCs are thought to be attractive for reinforcing polymers and increasing the hydrophilicity of nanocomposite materials.[32,33] It has been reported that CNCs have an effect on the reinforcement of several polymers such as poly(ethylene oxide), poly(methyl methacrylate), poly(propylene carbonate), poly(L-lactic acid), polyurethane, and cellulose acetate.[34,35] To the best of our knowledge, there is no article reporting the use of CNCs in pervaporation membranes. Therefore, the aim of this work was to explore the possibility of incorporating CNCs by blending with CTA and to investigate the effects of CNCs on PV performance membrane for water desalination.

2. EXPERIMENTAL SECTION

2.1. Chemicals and Materials. Cellulose triacetate (acetyl content 43−44%, molecular weight 966.845 g/mol) was purchased from ACROS (product of U.S.). Dimethyl sulfoxide (DMSO 99.5%, reagent) was obtained from ACROS (product of China). CNCs were purchased from CelluForce Inc. (Montreal, QC, Canada). Sodium chloride was obtained from ACROS (product Denmark) and was used as the solute in the feed. These chemicals were used without further purification.

2.2. Membrane Preparation. CTA and CTA/CNCs nanocomposite membranes were made by the solution casting method−solvent evaporation[36] using dimethyl sulfoxide (DMSO), which is an organic solvent with relatively low toxicity and environmental impact. The CNCs powder used had a particle size between 1 and 50 μm, a diameter between 2.3 and 4.5 nm, and a length range of 44−108 nm. Various CTA/CNCs dope solutions with 6 wt % CTA and different concentration of CNCs (0, 1, 2, 3, and 4 wt %) were prepared. The CNCs were first dispersed into DMSO as solvent; this was stirred for 3 h at room temperature until being homogenized. CTA polymer was then added and stirred for a further 15 h at 40 °C. These casting dopes were left for 2 h before centrifugation at 4000 rpm for 4 min to remove air bubbles. Then, these were cast on the glass plate using an automatic casting machine with a casting blade height of 200 μm, 150 μm, 100 μm, and 80 μm at room temperature and in a relative humidity range of 34−44%. A casting blade height of 80 μm was explored, but this appeared to be too thin because the membranes were leaky (Figure S4). The membranes on glass plates were heated in a vacuum oven for 4 h at 60 °C with 5 in. Hg pressure. The transparent membranes were obtained by peeling from the glass plate. The composition of the prepared casting dope and names of the fabricated membranes are listed in Table 1.

2.3. Characterization of the Membrane. *2.3.1. SEM Analysis.* The observations of the membrane surface and cross-

Table 1. Membrane Casting Dope Composition

membrane code	CTA (wt %)	CNCs (wt %)	DMSO (wt %)
CNCs 0%-CTA	6		94
CNCs 1%-CTA	6	1	93
CNCs 2%-CTA	6	2	92
CNCs 3%-CTA	6	3	91
CNCs 4%-CTA	6	4	90

DOI: 10.1021/acs.iecr.9b02106
Ind. Eng. Chem. Res. 2019, 58, 14340−14349

section morphologies were carried out using a XL30 FEG field-emission scanning electron microscope (FE-SEM, The Netherlands). The samples were mechanically fractured in liquid nitrogen before cross-section observation. Each sample was sputter-coated with a 1.5−2 nm Au layer before testing.

2.3.2. FTIR Analysis. The chemical composition of pristine CTA membranes and membranes prepared with addition of CNCs was analyzed by Fourier transform infrared spectroscopy (FTIR, PE spectrum 100 with a universal ATR sampling accessory).

2.3.3. AFM Analysis. The surface roughness of the prepared membranes was measured by atomic force microscopy (AFM, Bruker) in tapping mode, measured in air. The root-mean-square roughness (R_q), root average arithmetic roughness (R_a), and the mean difference between the highest peaks and lowest valleys (R_{max}) were used to analyze the membrane surface roughness for a scanning area of 1 μm × 1 μm for each sample.

2.3.4. Contact Angle Analysis. Contact angle measurements were conducted using a standard contact angle apparatus (Krüss GmbH Germany, model DSA 10-Mk2) to determine the degree of wettability. The measurements were performed using a drop-shape analysis software to study the video images of the water pendant drops. A syringe plunger was utilized for drop depositions on the surface of the membrane under study at room temperature. The liquid water volume was set at 2 μL at a rate of 24.79 μL/min.

2.3.5. Water Uptake Analysis. Water absorption of the membrane samples was measured by cutting the specimen in pieces of 2 cm × 2 cm, which were dried in an oven for 24 h at 105 °C. The dry specimens were weighed (W_d) and then placed in a container of feed solution (30 g/L NaCl in DI water) for 36 h. The wet specimens were weighed (W_w); results were expressed as a percentage of water absorption in relation with the dry weight of the specimens. The water uptake of the membrane was determined according to the following equation.

$$\text{water uptake}\ (\%) = \frac{W_w - W_d}{W_d} \times 100\% \quad (1)$$

2.3.6. Mechanical Properties. The modulus of elasticity and tensile strength of the samples were determined using a mini tensile/compression machine, model Instron 5943. At least four specimens were tested for each membrane type.

2.3.7. Evaluation of Membrane Separation Performance. A pervaporation study using the synthesized membranes was conducted using a Lab Test Cell Unit (Sulzer Chemtech) as shown in Figure 1. This system worked by applying a vacuum (Edwards two stage model E2M2, vacuum pressure 0.1−1 mbar) at the downstream location to enable separation by partial vaporization of the permeating component. The effective membrane surface area is 19.625 cm^2 (diameter = 5 cm) before being mounted onto the membrane cell unit. The pervaporation experiment was run for 2 h, and permeate was collected every 15 min and operated at 70 °C with a feed solution of 30 g/L NaCl in DI water at a feed flow rate of 80 L/h. The permeance (kg m^{-2} h^{-1}) was determined by the volume of permeate obtained over a given time interval and taking the effective area of the membrane. The salt rejections (R,%) were calculated from the following equation:

$$R(\%) = \left(1 - \frac{C_p}{C_f}\right) \times 100\% \quad (2)$$

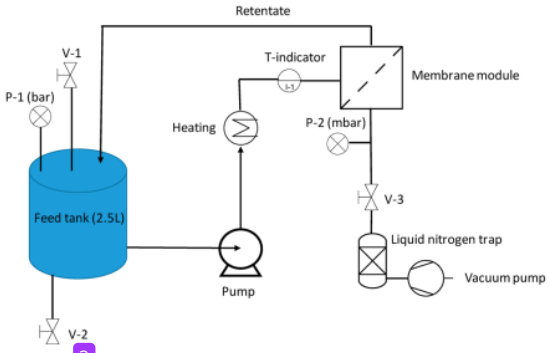

Figure 1. Schematic diagram of the experimental setup for pervaporation.

where C_p and C_f are the salinity in the permeate and feed solutions, respectively. The salinity of water was determined by an Adwa 8000-conductivity meter.

3. RESULTS AND DISCUSSION

3.1. Characterization and Membrane Performance of CTA/CNCs Nanocomposite Membrane. Smooth and transparent membranes were produced from CTA and CTA/CNCs casting dope solutions, using a casting blade height of 200 μm. Optimization of the membrane performance was explored by incorporating CNCs to increase the hydrophilicity of the membrane, which is thought to yield a higher water flux.

3.1.1. Membrane Compositions. FTIR spectroscopy spectra to characterize the chemical composition of the pristine CTA membrane and CTA/CNCs nanocomposite membranes are shown in Figure 2.

The most characteristic peaks for the pristine CTA membrane (Figure 2) are the peak at 1745 cm^{-1} corresponding to the C=O stretching, at 1364 cm^{-1} corresponding to the asymmetric bending of C−H, and at 1220 and 1035 cm^{-1} corresponding to C−O stretching and pyranose ring C−O−C stretching, respectively. Comparing the pristine CTA membrane to modified CTA by adding CNCs as in Figure 2, the absorption peaks at 3345 cm^{-1} become higher because of the presence of CNCs. The presence of CNCs on the CTA/CNCs nanocomposite membranes enhances the surface hydrophilicity because the peaks between 3500 and 3200 cm^{-1} are typical for OH stretching,[37,38] indicating the increase of oxygen-containing functional groups.

3.1.2. Effect of CNCs on Morphological Characteristics. Thermodynamics and kinetics are two important mechanism in the phase separation process of the polymer/solvent/nonsolvent system. The polymer precipitation behavior is related to thermodynamics while the exchange rate of the solvent/nonsolvent is related to the kinetics. Figure 3 shows that increasing the CNCs concentration generates an increasing viscosity. A higher viscosity prevents the exchange between solvent and nonsolvent during the phase inversion and decreases the driving force for membrane sedimentation, which leads to the formation of a dense skin layer. As a result, the morphology of the top layer is dominated by the kinetic mechanism from the viscosity of the dope solution.

The surface morphological features of CTA membranes in varying the CNCs content are shown in Figure 4. All

DOI: 10.1021/acs.iecr.9b02106
Ind. Eng. Chem. Res. 2019, 58, 14340−14349

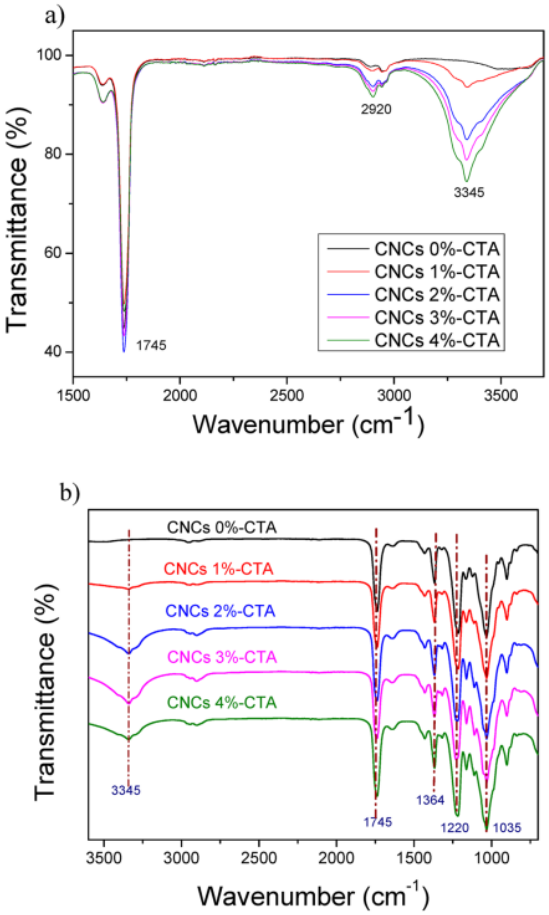

Figure 2. FTIR spectra of pristine CTA and CTA/CNCs nanocomposite membranes (a,b).

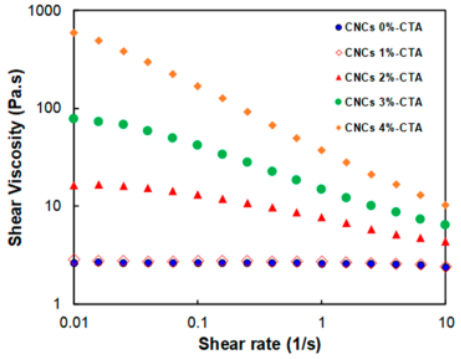

Figure 3. Viscosities of polymer casting solution with different CNCs concentrations.

membranes produced have dense surfaces, as shown in parts A1−E1, which is required for PV. Furthermore, the loading of hydrophilic CNCs will promote the mutual diffusion and speed up the gelation process.[39]

To characterize the surface roughness of the prepared membranes, AFM was used and the results are shown in Figure 4A2−E2 for different CTA/CNCs nanocomposite membranes. The AFM images clearly show significant differences in membrane surface roughness of pristine membrane and CTA/CNCs nanocomposite membranes. Membrane surface roughness is quantified using two parameters, i.e., R_q and R_a, with R_q as the root-mean-square average of height deviation taken from the mean image data plane and R_a the arithmetic average of the absolute values of the surface height deviations measured from the mean plane. The numerical values of these roughness parameters are summarized in Table 2. As the CNCs concentration in the polymer casting solution increases, the R_a value decreases gradually from 3.25 nm for pristine CTA membrane to 0.91 nm for membranes prepared from casting solution with CNCs loading of 3 wt %. The decreasing trend of R_a value indicates that the top surface of CTA/CNCs nanocomposites are smoother than that of pristine CTA membrane. The addition of hydrophilic CNCs into CTA casting solution affects the gelation process during membrane formation stage, which results in smooth surfaces in comparison to their pristine counterpart.[39] Moreover, the preferential location of CNCs on the top surface of the membranes could be another possible reason to explain why the nanocomposite membranes has reduced surface roughness. While CNCs cover the membrane surface homogeneously up to the concentration of 3 wt %, a further increase of CNCs to 4 wt % causes the slight increase of membrane surface roughness. This might due to an increase in membrane thickness at 4 wt % CNCs, which results in space enhancement on the membrane surface, causing uneven coverage of the membrane surface. Moreover, a higher viscosity of 4 wt % CNCs caused CNCs agglomeration on the membrane surface. Generally, the membrane surface roughness plays a significant role in the determination of the fouling tendency. A smooth surface typically can reduce the membrane fouling, because contaminants specifically concentrate in the valleys, block membrane pores, and therefore reduce the membrane permeability.[39]

The cross-sectional SEM images of the membranes were inspected to explore the effect of CNCs on the membrane microstructure. Figure 5 shows the cross section of pristine CTA membrane and CTA/CNCs nanocomposite membranes. The SEM image of the cross section of CTA/CNCs nanocomposite membranes shows that cellulose nanocrystals form a self-assembled structure. Normal evaporation of the CTA/CNCs casting dope causes the self-assembly of cellulosic crystals and creates a solid film with a specific structural organization (Figure 5b). Also, the image indicates a closely packed layer-by-layer structure due to the self-assembly of liquid crystalline materials and the antiparallel crystalline adjustment of the cellulose Iβ structure.[40,41]

3.1.3. Evaluation of Contact Angle and Water Uptake. Generally, the hydrophilicity of the membrane surface is one of the most important properties in this application. Figure 6a shows that increasing the CNCs concentration decreases the water contact angle, corresponding to an increased hydrophilicity of the membrane surface. Adding 4% CNCs into a CTA membrane yielded a slight decrease in membrane contact angle, from 57° (pristine CTA membrane) to about 50°.

The water uptake shown in Figure 6b significantly increases as the loading of CNCs increases. The increment of CNCs as filler leads to an increased water uptake since the hydrophilic

DOI: 10.1021/acs.iecr.9b02106
Ind. Eng. Chem. Res. 2019, 58, 14340−14349

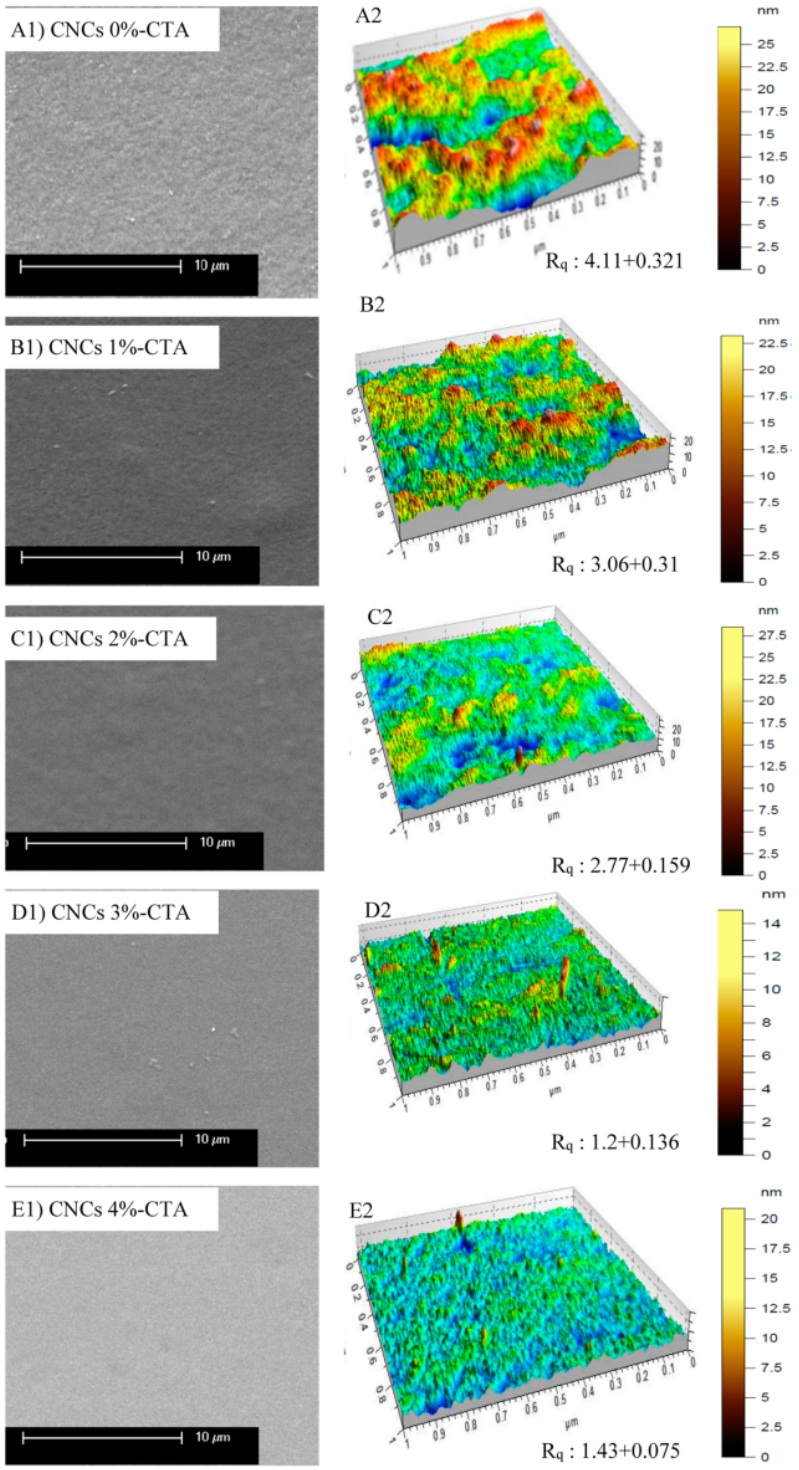

Figure 4. SEM images of the membrane surfaces (A1−E1) and three-dimensional AFM images of CTA membranes (A2−E2) at different CNCs contents. Scan size of 1 μm × 1 μm.

DOI: 10.1021/acs.iecr.9b02106
Ind. Eng. Chem. Res. 2019, 58, 14340−14349

Table 2. Surface Roughness Parameters of Pristine CTA and CTA/CNCs Nanocomposite Membranes

membrane	surface roughness parameters (average)		
	R_a (nm)	R_q (nm)	R_z (nm)
CNCs 0%-CTA	3.25 ± 0.27	4.11 ± 0.32	30.6 ± 3.21
CNCs 1%-CTA	2.39 ± 0.21	3.06 ± 0.31	32.45 ± 10.86
CNCs 2%-CTA	2.13 ± 0.78	2.77 ± 0.159	34.22 ± 11.4
CNCs 3%-CTA	0.91 ± 0.099	1.20 ± 0.136	13.52 ± 1.2
CNCs 4%-CTA	1.11 ± 0.05	1.43 ± 0.075	17.53 ± 3.26

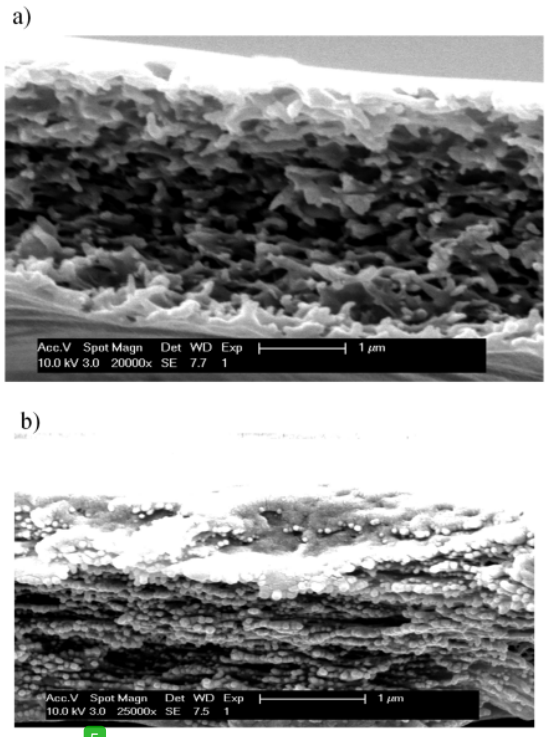

Figure 5. Cross-sectional SEM images: (a) pristine CTA membrane and (b) CNCs 3%-CTA nanocomposite membrane.

groups on the CNCs surface will interact strongly with the water molecules. The enhanced hydrophilicity of CTA/CNCs nanocomposite membranes can be attributed to the hydrophilic characteristic of CNCs due to the presence of OH and ester groups. The addition of CNCs contributed to a significant increase of O−H groups, as confirmed in Figure 2a. As a result, the presence of abundant hydroxyl groups of the CNCs increases the absorption of water molecules on the membrane surface through hydrogen bonding and van der Waals forces.[42−44] Cross-section images as shown in Figure 5b also indicates that some CNCs crystals attach into each layer on the sublayer of the membrane. This will in turn accelerate the water diffusion inside the membrane via hydrogen bonding interaction.

3.1.4. Mechanical Properties. The mechanical properties of PV membrane are considered for practical applications because the membrane is very thin. The tensile strength and Young modulus of the studied membranes are presented in Figure 7a.

The tensile strength of membranes improved from about 28.48 N mm^{-2} to 65.53 N mm^{-2}, while the Young modulus enhanced from 1.649 to 8.561 MPa with increasing CNCs content. The improvement of mechanical properties is especially associated with the adhered character of CNCs and the solid interaction between CNCs and the hydrophilic CTA. CNCs interact with the CTA polymer matrix through hydrogen bonding due to the abundance of hydroxyl groups in CNCs, as illustrated in Figure S5. As a result, the FTIR analysis of CTA/CNCs nanocomposite shows a higher peak at 2920 cm^{-1} than pristine CTA due to the increase of C−H groups from CNCs. However, the strength of the membrane decreased when 3% CNCs was loaded because the membrane thickness was not increasing, while the thickness increased from 8.10^{-3} mm to 10.10^{-3} mm when 4% CNCs were added (see Figure 7b).

3.2. Performance of CTA/CNCs Nanocomposite Membranes in Pervaporation. Figure 8 shows the effect of CNCs on the membrane water flux and NaCl rejection. The water flux increased dramatically from 2.16 to 7.98 kg m^{-2} h^{-1} while the NaCl rejection was maintained above 99.8% with increasing CNCs content up to 4%. The increase of water flux due to the presence of CNCs in the membrane affects the water transport by creating permeation pathways for selective species but providing a barrier for nonselective species. In the solution-diffusion mechanism, the solubility of the permeant

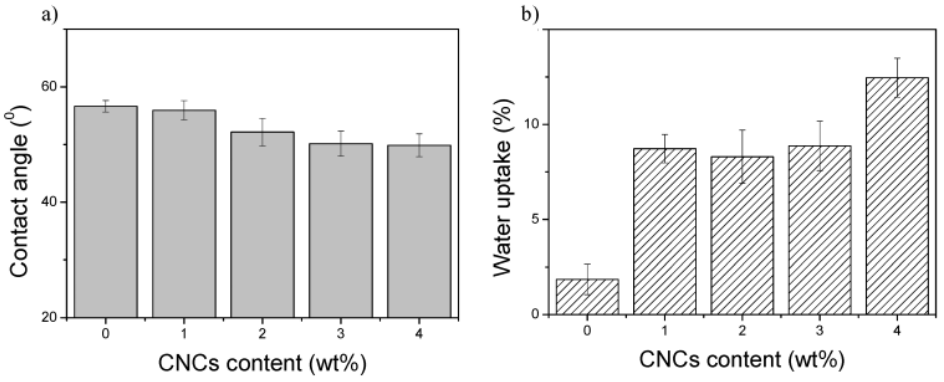

Figure 6. (a) Contact angle and (b) water uptake of the membranes at different CNCs contents.

DOI: 10.1021/acs.iecr.9b02106
Ind. Eng. Chem. Res. 2019, 58, 14340−14349

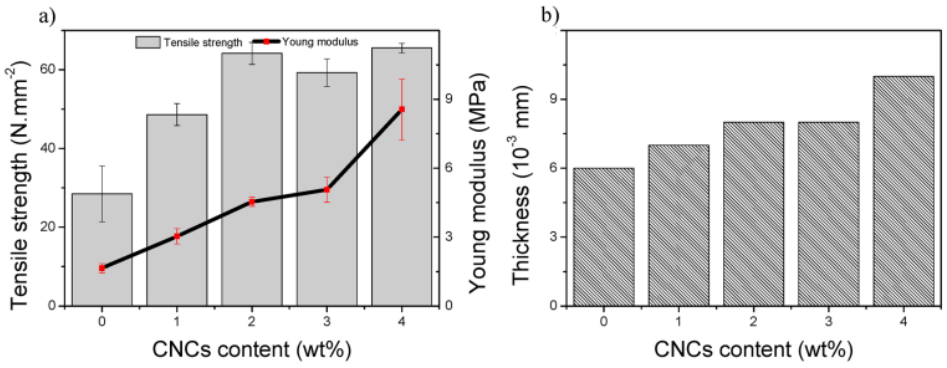

Figure 7. Mechanical properties (a) and membrane thickness (b) at different CNCs contents.

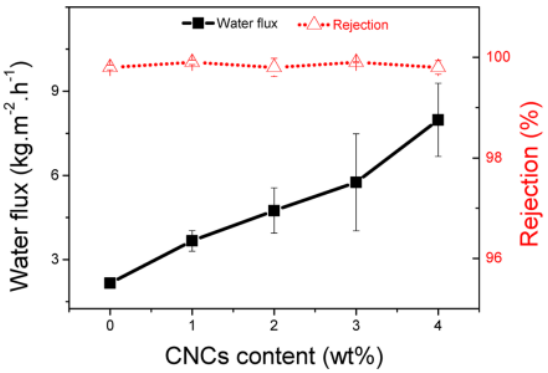

Figure 8. Membrane performance at different CNCs content.

into the membrane depends on the permeant solubility, which is influenced by the interaction between the permeant and the membrane material.[45] CNCs have a dual effect on the membrane permeability, i.e., an improvement of the membrane hydrophilicity (Figure 6) and a change in membrane morphology, as presented in Figures 4 and 5. The addition of CNCs also result in a more expressed hydrophilicity of the CTA/CNCs nanocomposite membrane surface due to the rise of hydroxyl groups, which promote hydrogen bonding formation and thereby more water molecules can be attracted.

The presence of CNCs on the membrane resulted in an increasing water flux but did not decrease the NaCl rejection. This might be because of the unique structure of the membrane. The self-assembled structure on the membrane produced an ordered structure which might allow one to maintain the selectivity.

3.3. Effect of Temperature and Feed Concentration on Membrane Performance. Operating conditions such as temperature and feed concentration will affect the membrane performance of pervaporation. Figure 9a shows the desalination performances of CNCs 3%-CTA nanocomposite membranes at temperatures 30 and 70 °C. It was almost a triple increase of water flux (from 1.9 kg m^{-2} h^{-1} to 5.8 kg m^{-2} h^{-1}) when the temperature was enhanced from 30 to 70 °C. The increment of water flux because the vapor pressure in the feed side was escalated generated the driving force, which led to a boost in the water flux. Furthermore, rising the feed temperature will promote a higher water flux because water molecules will diffuse easily through the membranes.[46]

The effect of feed concentration on the desalination performance was also investigated for feed solution in the range of 30−90 g/L, and the results were described in Figure 9b. Increasing the NaCl concentration in the feed solution led to a water flux decline as reduced water concentration in the feed will decrease water sorption at the membrane interface. Although water flux was affected by the feed concentration, NaCl rejection was maintained above 99.9% because the

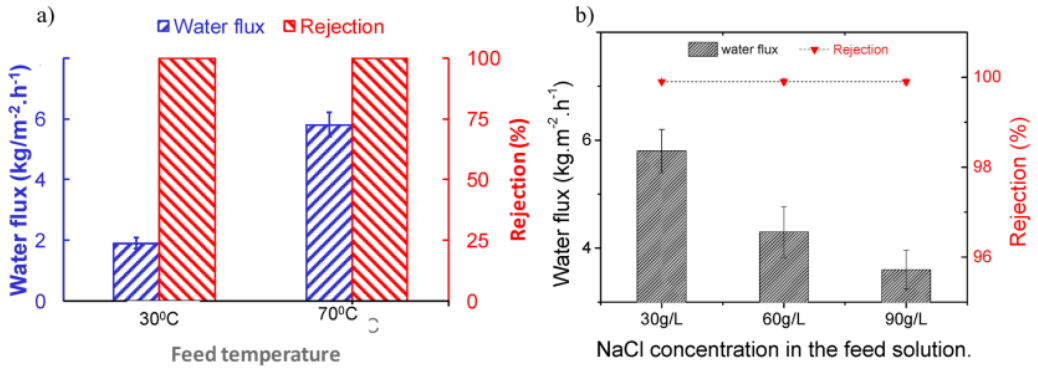

Figure 9. Effect of temperature (a) and feed concentration (b) on the CNC 3%-CTA nanocomposite membrane performance.

DOI: 10.1021/acs.iecr.9b02106
Ind. Eng. Chem. Res. 2019, 58, 14340−14349

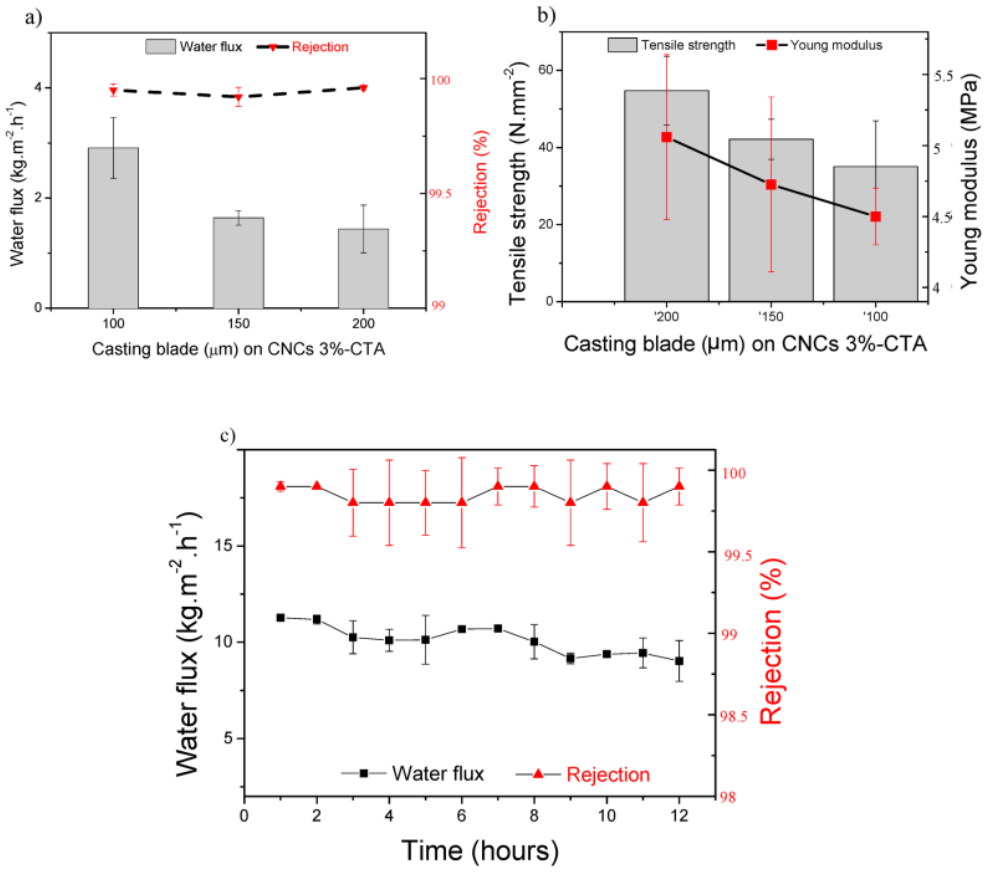

Figure 10. CNC 3%-CTA membrane performance at different heights of the casting blade (a), mechanical property of CNCs 3%-CTA membrane (b), and performance of the CNC 3%-CTA nanocomposite membrane as a function of exposure time at 100 μm of the casting blade height (c).

structure of the CTA/CNCs nanocomposite membrane prevented the NaCl penetration through the membrane.

3.4. Effect of Casting Blade Height on Membrane Performance. Figure 10a shows that a reduction of the membrane thickness can significantly improve the PV performance. The water flux increased from 5.75 kg m^{-2} h^{-1} to 11.68 kg m^{-2} h^{-1} when the casting blade height was reduced from 200 to 100 μm while the NaCl rejection remained at least at 99.9%. As a result, the membrane thickness reduced from 10 to 6 μm. The membrane thickness affects the water flux due to transport of water molecules through the membrane by solution-diffusion.[47] The mechanism illustrates that water molecules will be absorbed into the membrane at the feed side, followed by diffusion due to a chemical potential difference across the membrane, then desorbed at the permeate side. This is modeled by Fick's law by describing that the flux of a component through the membrane is inversely proportional to the membrane thickness.[47] In spite of the decrease of the membrane tensile strength from 54.72 N mm^{-2} to 35.07 N mm^{-2} when the thickness was reduced from 200 to 100 μm height of casting blade (see Figure 10b), the membrane performance during 12 h of pervaporation shown in Figure 10c suggests that a casting height of 100 μm results in a positive performance stability.

4. CONCLUSIONS

An enhanced water flux of a PV membrane for water desalination was successfully achieved by blending 3% CNCs in a CTA casting dope via solution casting. The incorporation of CNCs in CTA membranes not only changed the membrane structure (decreased membrane surface roughness and declined contact angle due to the abundant hydroxyl groups of CNCs) but also improved the mechanical strength of the membranes. For a membrane made of CNCs 3%-CTA, the water flux was tripled compared to a pristine CTA membrane (from 2.16 kg m^{-2} h^{-1} to 5.76 kg m^{-2} h^{-1}). Furthermore, the flux was further increased by a factor of 6 (11.68 kg m^{-2} h^{-1}) by a decreased casting blade height (from 200 to 100 μm), while the NaCl rejection maintained at least 99.9%. In addition, the CNCs 3%-CTA membrane prepared with a casting blade of 100 μm gave a positive performance for a 12 h separation process. The results demonstrated that the newly developed CNCs 3%-CTA blending membrane is a promising candidate for a PV membrane.

■ ASSOCIATED CONTENT

Supporting Information

The Supporting Information is available free of charge on the ACS Publications website at DOI: 10.1021/acs.iecr.9b02106.

DOI: 10.1021/acs.iecr.9b02106
Ind. Eng. Chem. Res. 2019, 58, 14340−14349

Figure S1, pristine 6% CTA membrane performance at different temperatures; Figure S2, contact angles of CTA membranes at different polymer concentrations; Figure S3, water flux and rejection performances of CTA membranes; Figure S4, membrane performances of the CNCs 3%-CTA nanocomposite membranes as a function of exposure time; and Figure S5, illustration of the hydrogen bonding of the hydroxyl group in CNCs with CTA (PDF)

AUTHOR INFORMATION

Corresponding Author

*E-mail: bart.vanderbruggen@kuleuven.be.

ORCID

Indah Prihatiningtyas: 0000-0002-3713-9722

Author Contributions

The manuscript was written through contributions of all authors. All authors have given approval to the final version of the manuscript.

Notes

The authors declare no competing financial interest.

ACKNOWLEDGMENTS

This work was supported by the Indonesia Endowment Fund for Education (LPDP). We thank Ani Vananroye (KU Leuven) for measuring the viscosity and Yusak Hartanto for the fruitful discussions (KU Leuven).

ABBREVIATIONS

PV = pervaporation
CNCs = cellulose nanocrystal
CTA = cellulose triacetate
MSF = multistage flash distillation
MED = multiple effect distillation
VC = vapor compression
HDH = humidification-dehumidification
GO = graphene oxide
CNT = carbon nanotubes
MWNT = multiwalled carbon nanotube
SEM = scanning electron microscope
FTIR = Fourier-transform infrared spectroscopy
AFM = atomic force microscope.

REFERENCES

(1) Elimelech, M.; Phillip, W. A. The Future of Seawater Desalination: Energy, Technology, and the Environment. *Science* **2011**, *333*, 712−717.
(2) Sivakumar, B. Water Crisis: From Conflict to Cooperation an Overview. *Hydrol. Sci. J.* **2011**, *56* (4), 531−552.
(3) Garcia-Rodriguez, L. Renewable Energy Applications in Desalination: State of the Art. *Sol. Energy* **2003**, *75* (5), 381−393.
(4) Wang, Q.; Li, N.; Bolto, B.; Hoang, M.; Xie, Z. Desalination by Pervaporation: A Review. *Desalination* **2016**, *387*, 46−60.
(5) Charcosset, C. A Review of Membrane Processes and Renewable Energies for Desalination. *Desalination* **2009**, *245* (1), 214−231.
(6) Figoli, A.; Santoro, S.; Galiano, F.; Basile, A. *Pervaporation Membranes: Preparation, Characterization, and Application*; Elsevier Ltd., 2015.
(7) Van der Bruggen, B.; Luis, P. *Pervaporation*; Elsevier Ltd., 2014.
(8) Xie, Z.; Ng, D.; Hoang, M.; Zhang, J.; Gray, S. Study of Hybrid PVA/MA/TEOS Pervaporation Membrane and Evaluation of Energy Requirement for Desalination by Pervaporation. *Int. J. Environ. Res. Public Health* **2018**, *15* (9), 1913.
(9) Elma, M.; Yacou, C.; Wang, D. K.; Smart, S.; Diniz da Costa, J. C. Microporous Silica Based Membranes for Desalination. *Water* **2012**, *4* (3), 629−649.
(10) Nigiz, F. U.; Hilmioglu, N. D. Pervaporative Desalination of Seawater by Using Composite and Blended Poly(Vinyl Alcohol) Membranes. *Desalin. Water Treat.* **2016**, *57* (11), 4749−4755.
(11) Huth, E.; Muthu, S.; Ruff, L.; Brant, J. A. Feasibility Assessment of Pervaporation for Desalinating High-Salinity Brines. *J. Water Reuse Desalin.* **2014**, *4* (2), 109−124.
(12) Feng, X.; Huang, R. Y. M. Pervaporation with Chitosan Membranes. I. Separation of Water from Ethylene Glycol by a Chitosan/Polysulfone Composite Membrane. *J. Membr. Sci.* **1996**, *116* (1), 67−76.
(13) Korngold, E.; Korin, E.; Ladizhensky, I. Water Desalination by Pervaporation with Hollow Fiber Membranes. *Desalination* **1996**, *107* (2), 121−129.
(14) Yu, Y.; Wu, Q. Y.; Liang, H. Q.; Gu, L.; Xu, Z. K. Preparation and Characterization of Cellulose Triacetate Membranes via Thermally Induced Phase Separation. *J. Appl. Polym. Sci.* **2017**, *134* (6), 1−10.
(15) Ong, R. C.; Chung, N. T.-S.; de Wit, J. S.; Helmer, B. J. Novel Cellulose Ester Substrates for High Performance Flat-Sheet Thin-Film Composite (TFC) Forward Osmosis (FO) Membranes. Journal of Membrane Science. *J. Membr. Sci.* **2015**, *473*, 63−71.
(16) Majeed, T.; Lotfi, F.; Phuntsho, S.; Yoon, J. K.; Kim, K.; Shon, H. K. Performances of PA Hollow Fiber Membrane with the CTA Flat Sheet Membrane for Forward Osmosis Process. *Desalin. Water Treat.* **2015**, *53* (7), 1744−1754.
(17) Zhang, X.; Ning, Z.; Wang, D. K.; Diniz da Costa, J. C. Processing Municipal Wastewaters by Forward Osmosis Using CTA Membrane. *J. Membr. Sci.* **2014**, *468*, 269−275.
(18) Mi, B.; Elimelech, M. Chemical and Physical Aspects of Organic Fouling of Forward Osmosis Membranes. *J. Membr. Sci.* **2008**, *320* (1−2), 292−302.
(19) Chen, X.; Xu, J.; Lu, J.; Shan, B.; Gao, C. Enhanced Performance of Cellulose Triacetate Membranes Using Binary Mixed Additives for Forward Osmosis Desalination. *Desalination* **2017**, *405*, 68−75.
(20) Chen, K.; Xiao, C.; Liu, H.; Li, G.; Meng, X. Structure Design on Reinforced Cellulose Triacetate Composite Membrane for Reverse Osmosis Desalination Process. *Desalination* **2018**, *441*, 35−43.
(21) You, M.; Yin, J.; Sun, R.; Cao, X.; Meng, J. Water/Salt Transport Properties of Organic/Inorganic Hybrid Films Based on Cellulose Triacetate. *J. Membr. Sci.* **2018**, *563*, 571−583.
(22) Teow, Y. H.; Mohammad, A. W. New Generation Nanomaterials for Water Desalination: A Review. *Desalination* **2019**, *451*, 2−17.
(23) Ying, Y.; Ying, W.; Li, Q.; Meng, D.; Ren, G.; Yan, R.; Peng, X. Recent Advances of Nanomaterial-Based Membrane for Water Purification. *Appl. Mater. Today* **2017**, *7*, 144−158.
(24) Asempour, F.; Emadzadeh, D.; Matsuura, T.; Kruczek, B. Synthesis and Characterization of Novel Cellulose Nanocrystals-Based Thin Film Nanocomposite Membranes for Reverse Osmosis Applications. *Desalination* **2018**, *439*, 179−187.
(25) Jhaveri, J. H.; Murthy, Z. V. P. *Nanocomposite Membranes*; Elsevier Inc., 2016.
(26) Lau, W. J.; Gray, S.; Matsuura, T.; Emadzadeh, D.; Paul Chen, J.; Ismail, A. F. A Review on Polyamide Thin Film Nanocomposite (TFN) Membranes: History, Applications, Challenges and Approaches. *Water Res.* **2015**, *80*, 306−324.
(27) Ng, L. Y.; Mohammad, A. W.; Leo, C. P.; Hilal, N. Polymeric Membranes Incorporated with Metal/Metal Oxide Nanoparticles: A Comprehensive Review. *Desalination* **2013**, *308*, 15−33.
(28) Bottero, J. Y.; Rose, J.; Wiesner, M. R. Nanotechnologies: Tools for Sustainability in a New Wave of Water Treatment Processes. *Integr. Environ. Assess. Manage.* **2006**, *2* (4), 391−395.
(29) Goh, P. S.; Ismail, A. F.; Matsuura, T. Perspective and Roadmap of Energy-Efficient Desalination Integrated with Nanomaterials. *Sep. Purif. Rev.* **2018**, *47* (2), 124−141.

DOI: 10.1021/acs.iecr.9b02106
Ind. Eng. Chem. Res. 2019, 58, 14340−14349

(30) Zhang, L.-Q.; Niu, B.; Yang, S.-G.; Huang, H.-D.; Zhong, G.-J.; Li, Z.-M. Simultaneous Preparation and Dispersion of Regenerated Cellulose Nanoparticles Using a Facile Protocol of Dissolution−Gelation−Isolation−Melt Extrusion. *ACS Sustainable Chem. Eng.* **2016**, *4* (5), 2470−2478.
(31) Tan, C.; Peng, J.; Lin, W.; Xing, Y.; Xu, K.; Wu, J.; Chen, M. Role of Surface Modification and Mechanical Orientation on Property Enhancement of Cellulose Nanocrystals/Polymer Nanocomposites. *Eur. Polym. J.* **2015**, *62*, 186−197.
(32) Goetz, L.; Mathew, A.; Oksman, K.; Gatenholm, P.; Ragauskas, A. J. A Novel Nanocomposite Film Prepared from Crosslinked Cellulosic Whiskers. *Carbohydr. Polym.* **2009**, *75* (1), 85−89.
(33) Ganster, J.; Fink, H. P. Novel Cellulose Fiber Reinforced Thermoplastic Materials. *Cellulose* **2006**, *13* (3), 271−280.
(34) Zhou, J.; Chen, J.; He, M.; Yao, J. Cellulose Acetate Ultrafiltration Membranes Reinforced by Cellulose Nanocrystals: Preparation and Characterization. *J. Appl. Polym. Sci.* **2016**, *133* (39), 1−7.
(35) Zhang, Z.; Wu, Q.; Song, K.; Ren, S.; Lei, T.; Zhang, Q. Using Cellulose Nanocrystals as a Sustainable Additive to Enhance Hydrophilicity, Mechanical and Thermal Properties of Poly-(Vinylidene Fluoride)/Poly(Methyl Methacrylate) Blend. *ACS Sustainable Chem. Eng.* **2015**, *3* (4), 574−582.
(36) Altinkaya, S. A.; Yenal, H.; Ozbas, B. Membrane Formation by Dry-Cast Process: Model Validation through Morphological Studies. *J. Membr. Sci.* **2005**, *249* (1−2), 163−172.
(37) Sofla, M R. K.; Brown, R J; Tsuzuki, T; Rainey, T J A Comparison of Cellulose Nanocrystals and Cellulose Nanofibres Extracted from Bagasse Using Acid and Ball Milling Methods. *Adv. Nat. Sci.: Nanosci. Nanotechnol.* **2016**, *7* (3), 035004.
(38) Akhlaghi, S. P.; Zaman, M.; Mohammed, N.; Brinatti, C.; Batmaz, R.; Berry, R.; Loh, W.; Tam, K. C. Synthesis of Amine Functionalized Cellulose Nanocrystals: Optimization and Characterization. *Carbohydr. Res.* **2015**, *409*, 48−55.
(39) Lv, J.; Zhang, G.; Zhang, H.; Yang, F. Exploration of Permeability and Antifouling Performance on Modified Cellulose Acetate Ultrafiltration Membrane with Cellulose Nanocrystals. *Carbohydr. Polym.* **2017**, *174*, 190−199.
(40) Abraham, E.; Kam, D.; Nevo, Y.; Slattegard, R.; Rivkin, A.; Lapidot, S.; Shoseyov, O. Highly Modified Cellulose Nanocrystals and Formation of Epoxy-Nanocrystalline Cellulose (CNC) Nanocomposites. *ACS Appl. Mater. Interfaces* **2016**, *8* (41), 28086−28095.
(41) Larsson, P. T.; Hult, E.-L.; Wickholm, K.; Pettersson, E.; Iversen, T. CP/MAS 13C-NMR Spectroscopy Applied to Structure and Interaction Studies on Cellulose I. *Solid State Nucl. Magn. Reson.* **1999**, *15* (1), 31−40.
(42) Zhao, J. L.; Zhang, Y. Z.; Lin, L. G.; Ding, X. L.; Zhao, L. Z.; Ye, H.; Li, H. Preparation and Characterization of Novel PES/SPES Blend Ultrafiltration Membranes. *J. Tianjin Polytech. Univ.* **2013**, *32* (3), 1−7.
(43) Jayalakshmi, A.; Rajesh, S.; Senthilkumar, S.; Hari Sankar, H. S.; Mohan, D. Preparation of Poly (Isophthalamide-Graft-Methacrylamide) and Its Utilization in the Modification of Cellulose Acetate Ultrafiltration Membranes. *J. Ind. Eng. Chem.* **2014**, *20* (1), 133−144.
(44) Mohamed, M. A.; Salleh, W. N. W.; Jaafar, J.; Ismail, A. F.; Abd. Mutalib, M.; Jamil, S. M. Feasibility of Recycled Newspaper as Cellulose Source for Regenerated Cellulose Membrane Fabrication. *J. Appl. Polym. Sci.* **2015**, *132* (43), 42684.
(45) Roy, S.; Singha, N. R. Polymeric Nanocomposite Membranes for next Generation Pervaporation Process: Strategies, Challenges and Future Prospects. *Membranes (Basel, Switz.)* **2017**, *7* (3), 53.
(46) Hoang, M.; Gray, S.; Ng, D.; Xie, Z.; Duong, T. Separation of Aqueous Salt Solution by Pervaporation through Hybrid Organic−inorganic Membrane: Effect of Operating Conditions. *Desalination* **2011**, *273* (1), 220−225.
(47) Lonsdale, H. K.; Merten, U.; Riley, R. L. Transport Properties of Cellulose Acetate Osmotic Membranes. *J. Appl. Polym. Sci.* **1965**, *9* (4), 1341−1362.

DOI: 10.1021/acs.iecr.9b02106
Ind. Eng. Chem. Res. 2019, 58, 14340−14349

110th Anniversary: Cellulose Nanocrystals as Organic Nanofillers for Cellulose Triacetate Membranes Used for Desalination by Pervaporation

ORIGINALITY REPORT

21%	7%	21%	11%
SIMILARITY INDEX	INTERNET SOURCES	PUBLICATIONS	STUDENT PAPERS

PRIMARY SOURCES

1	Submitted to Associatie K.U.Leuven Student Paper	6%
2	Aristotelis Kamtsikakis, Sara McBride, Justin O. Zoppe, Christoph Weder. "Cellulose Nanofiber Nanocomposite Pervaporation Membranes for Ethanol Recovery", ACS Applied Nano Materials, 2021 Publication	6%
3	Indah Prihatiningtyas, Yi Li, Yusak Hartanto, Anja Vananroye, Nico Coenen, Bart Van der Bruggen. "Effect of solvent on the morphology and performance of cellulose triacetate membrane/cellulose nanocrystal nanocomposite pervaporation desalination membranes", Chemical Engineering Journal, 2020 Publication	4%
4	Submitted to Universidad Nacional de Colombia Student Paper	3%

5	Indah Prihatiningtyas, Gebrehiwet Abrham Gebreslase, Bart Van der Bruggen. "Incorporation of Al2O3 into cellulose triacetate membranes to enhance the performance of pervaporation for desalination of hypersaline solutions", Desalination, 2020 Publication	2%

Exclude quotes	On	Exclude matches	< 2%
Exclude bibliography	On		